Interfacial Tension Measurements of the (H_2O + CO_2) System at Elevated Pressures and Temperatures†

Apostolos Georgiadis, Geoffrey Maitland, J. P. Martin Trusler, and Alexander Bismarck*

Department of Chemical Engineering and Chemical Technology, Imperial College London, London SW7 2AZ, United Kingdom

Interfacial tension measurements are reported for the (H_2O + CO_2) system at pressures of (1 to 60) MPa and temperatures of (298 to 374) K. The pendant drop method was implemented using a high-pressure apparatus consisting of a view cell, fitted with a high-pressure capillary tube for creating pendant H_2O drops in the CO_2 bulk phase. The reported results have a relative standard deviation in most cases of less than 1.0 % and are in good agreement with literature values at low pressures. However, at higher pressures (up to 45 MPa), there is a significant scatter in the published data; the reasons for this are discussed. Measurements in the present work extend the pressure range of available data up to pressures of 60 MPa.

Introduction

CO_2 has been identified as one of the long-lived greenhouse gases (GHGs) emitted by human activity, along with CH_4, N_2O, and hydrofluorocarbons. Although CO_2 has a lower global warming potential (GWP) than these other gases, it remains the highest in terms of both emissions and impact.[1] For direct comparison, the unit of equivalent CO_2 emissions is used, which is the product of the GWP and the emissions of each GHG. In 2004, the CO_2 produced from fossil fuel burning accounted for 56.6 % of the world's total annual equivalent CO_2 emissions. These have in turn grown since 1970 by 70 %.[2] Carbon capture and storage[3,4] appear to be an attractive approach for mitigating CO_2 and are projected to play a major role in emissions reduction.[3]

Sequestration can be achieved by the injection of CO_2 in underground formations at depths of approximately 800 m or more. Assuming a geothermal gradient of 0.03 $K \cdot m^{-1}$ and hydrostatic pressure,[5] the conditions at these depths would be $T \geq 310$ K and $p \geq 8$ MPa. Pure CO_2 would therefore be in a supercritical state[6] with a density $\rho \geq 300$ $kg \cdot m^{-3}$. Storage would be feasible as long as buoyancy forces can be balanced by capillary forces, trapping CO_2 in rock pores, and/or CO_2 is retained below an impermeable cap rock.

Storage formations can be deep saline aquifers and depleted oil or gas reservoirs.[3] A range of trapping mechanisms apply in aquifer formations: in the medium-term (hundreds of years) by dissolution of CO_2 in the aqueous phase with consequent sinking of the denser carbonated water and in the long-term (millions of years) by mineral trapping with dissolved CO_2 precipitating in the presence of ionic species to form calcium, magnesium, and iron carbonates.[5] However, in the short-term (decades) storage of CO_2 in porous reservoirs or aquifer rocks must rely on capillary trapping—injection into micrometer-sized pores where interfacial tension causes the nonwetting CO_2 phase to be retained between narrow pore throats.

Ocean storage is also an option that has been considered, since the (H_2O + CO_2) system, at appropriate depths, can form hydrates and sink to the ocean floor. The effects of CO_2 dissolution on the pH of the ocean and consequently to the ecosystem are however uncertain.[7−9] CO_2 is also used as a process fluid in oil and gas reservoirs[10] for enhanced oil recovery (EOR) or in coal beds for enhanced coal bed methane processes.[11] In EOR processes, CO_2 can be trapped by capillary forces in the porosity of the reservoir after displacing the in situ oil or gas, so liberating at the same time useful hydrocarbons.

The main cause of capillary trapping is ultimately linked to the interfacial properties of CO_2 with the existing fluids in the reservoir, mainly brine and hydrocarbons. The interfacial tension, γ, of CO_2 with mixtures representative of the fluids in underground formations is an important thermophysical property for the design of such processes. The data available in the literature are limited in extent and accuracy, especially at elevated pressures and temperatures. Such high-pressure, high-temperature (HPHT) interfacial tension data for the (H_2O + CO_2) system are required in reservoir flow models to extend their predictive capability over a wide pressure and temperature range.

Two main methods for measuring interfacial tension at elevated pressures are reported in the literature: the pendant drop method, using either selected plane (SP)[12] or drop shape analysis (DSA)[13] and the capillary rise method.[14] The DSA of pendant drops has been applied in this work. The theoretical background for the determination of interfacial tension from DSA is described extensively by Song and Springer.[13,15]

Several references on interfacial tension measurements for the (H_2O + CO_2) system are available. A controversy, however, in the determination of a unique static interfacial tension is apparent when reported results from different authors are compared. Tewes and Boury[16] have focused extensively on the time dependence of the system by measuring pendant drops for as long as 100 000 s. Their results show a significant decrease of interfacial tension over this period which is attributed by the authors to molecular reorganization at the interface. da Rocha et al.,[17] Chun and Wilkinson,[18] and Chalbaud et al.[19] also allowed time for equilibrium by leaving the two phases in contact for "1 h", "days", and "1000 s", respectively. On the other hand, Hebach et al.,[20] having also noticed that the interfacial tension decreases over extended time periods, link

† Part of the "Sir John S. Rowlinson Festschrift".

* To whom correspondence should be addressed. E-mail: a.bismarck@imperial.ac.uk.

10.1021/je100198g
Published on Web 05/24/2010

Table 1. Different Approaches to Interfacial Tension Measurement of the (H_2O + CO_2) System in the Literature[a]

							agreement		
authors	year	method	H_2O (1)	CO_2 (2)	saturation	waiting	G	L	SC
Hough et al.[41]	1959	PD	P	P	NO	10 s	*B*		*D*
Massoudi and King[27]	1974	CR	C	P	NO		*A*		
Jho et a.[39]	1978	CR	C	P		"minutes"	*A*		
Chun and Wilkinson[18]	1995	CR		P		"days"	*A*	*B*	*C*
Wesch et al.[40]	1997	PD-SP	P	P	NO		*B*	*D*	*D*
da Rocha et al.[17]	1999	PD-DSA	P	P	CP	1 h			*D*
Hebach et al.[20]	2002	PD-DSA	P	P	NO	(10 to 15) min	*A*	*A*	*A*
Tewes and Boury[16]	2004	PD-DSA			SV-12h	60 000 s			*D*
Park et al.[23]	2005	CR	mR-H	P	NO	(5 to 7) s	*B*	*D*	*C*
Chiquet et al.[25]	2006	PD-DSA	M	M	MV				*B*
Chalbaud et al.[19]	2006	PD-DSA	S−W	P	SV	1000 s		*B*	*C*
Akutsu et al.[24]	2007	PD-SP	P	P	CP		*B*		*C*
Bachu and Bennion[26]	2008	PD-DSA	M	M	MV		*B*	*B*	*D*
Sutjiadi-Sia et al.[30]	2008	PD-DSA			NO		*C*		*D*

[a] PD = pendant drop, CR = capillary rise, DSA = drop shape analysis, SP = selected plane, P = pure compound densities, M = measured densities, C = constant densities, mR-H = modified Rackett-Hankinson modeled densities, S−W = Søreide and Whitson modeled densities, CP = circulation pump, SV = static vessel, MV = mixing vessel. The literature values have been compared with the present work in three regions of bulk CO_2 (2) states: G = gaseous, L = liquid, and SC = supercritical, where the agreement is $A < 5$ %, 5 % < $B < 10$ %, 10 % < $C < 20$ %, or 20 % < *D*.

this to "aging effects" due to factors other than phase equilibration and assume that static interfacial tension can only be measured within the initial plateau which is reached during the first (10 to 15) min. This is supported to some extent by Zappe et al.[21] and Kögel[22] who have measured diffusion times of supercritical CO_2 in H_2O drops, both showing that the time needed for the equilibrium concentration of CO_2 in typical H_2O drops (approximate radius of 2 mm) to develop is in the range of (200 to 300) s. Time dependence as well as equilibrium values of interfacial tension are largely affected by impurities which are inherently present in trace amounts in any high-pressure apparatus. In fact the effect of appropriate surfactants for the (H_2O + CO_2) system are reported by Park et al.,[23] Tewes and Boury,[16] Akutsu et al.,[24] and da Rocha et al.[17]

Another important factor for the correct determination of interfacial tension is how the temperature is measured. Hebach et al.[20] showed that the minimum values observed near the dew point of the CO_2-rich phase, reported by Chun and Wilkinson[18] and Park et al.,[23] were actually due to a temperature measurement error.

The determination of the density difference between the two phases is also approached in various ways, something which has been associated with disagreement between the data reported by different authors. Chiquet et al.[25] and Bachu and Bennion[26] both measured the actual densities of the two phases by using a vibrating-tube densimeter. Chiquet et al.[25] concluded that the approximation of using pure compound densities, as followed by most authors, is indeed good for the (H_2O + CO_2) system. However, at pressures near that of density inversion at a temperature of 308 K, where the inversion pressure is 53.6 MPa, the density difference of the pure compounds, $\Delta\rho$, can be up to 1.7 times smaller than the actual one, as noted by the same authors. This results in an underestimation of the interfacial tension by up to 40 %. The values reported by Chun and Wilkinson[18] and Park et al.[23] at conditions of liquid CO_2 are significantly lower than the values of Chiquet et al.,[25] Massoudi and King,[27] and Hebach et al.[20] The fact that Chun and Wilkinson[18] and Park et al.[23] used the capillary rise technique instead of the pendant drop method does not seem to be the reason for this as Massoudi and King[27] also used the same technique and reported values very close to Hebach et al.[20] and Chiquet et al.[25] who used the pendant drop method. Chiquet et al.[25] ascribe this ambiguity to the use of pure compound densities instead of measured densities of the saturated fluids; however, Hebach et al.[20] used the densities of the pure compounds, and Massoudi and King[27] even assumed the density of H_2O to remain constant, yet the values of both agree with Chiquet et al.[25] Table 1 summarizes the approaches used by several different authors with respect to these factors. This work has been designed to resolve some of these discrepancies and to extend the range of HPHT measurements of interfacial tension available for the (H_2O + CO_2) system.

Experimental Section

Materials. The CO_2 used was of CP grade, supplied by BOC, with a mole fraction purity > 0.99995. The H_2O used was purified deionized water with better specifications than double-distilled water (electrical conductivity < 15 $\mu S \cdot cm^{-1}$). Hexane (BDH, Hull, UK), isopropanol (Sigma-Aldrich, Dorset, UK), and toluene (Sigma-Aldrich, Dorset, UK) used in this work for cleaning purposes were of mole fraction purities > 0.95, 0.999, and 0.999, respectively.

High-Pressure Apparatus. For the purpose of interfacial tension measurements at elevated pressures and temperatures, a custom-designed high-pressure view cell was used. The apparatus (Eurotechnica GmbH, model PD-E700 LL, Bargteheide, Germany) was designed to hold pressures up to 70 MPa at temperatures up to 473 K. A schematic diagram of the apparatus is shown in Figure 1.

The high-pressure view cell is indicated in Figure 1 as "VC" and was connected by means of 3.2 mm o.d. high-pressure tubing with two manual pressure generators (PG1 and PG2), each of 30 cm^3 capacity. These were used to introduce different fluids to the system, each from their respective storage tank (T1 and T2). The view cell was a hollow cylindrical vessel with flat ends made from AISI type 660 stainless steel. It had four fluid ports equally spaced around the circumference in the middle of the cell, allowing for high-pressure tubing connections. The two flat ends were fitted with 36 mm diameter glands which held in place the assemblies bearing the sapphire windows. The metal-to-metal faces were sealed by means of PTFE O-rings, while the metal-to-sapphire faces were sealed with a Poulter-type seal (unsupported area principle).[28,29] The inner volume of the view cell was 24 cm^3. The line connected to valve "G" in Figure 1 was used for introducing CO_2 to the view cell via a high-pressure automatic syringe pump (Teledyne Isco, model 100DM, Lincoln, USA). The latter was filled with CO_2 through a 2 μm line filter for particulate removal.

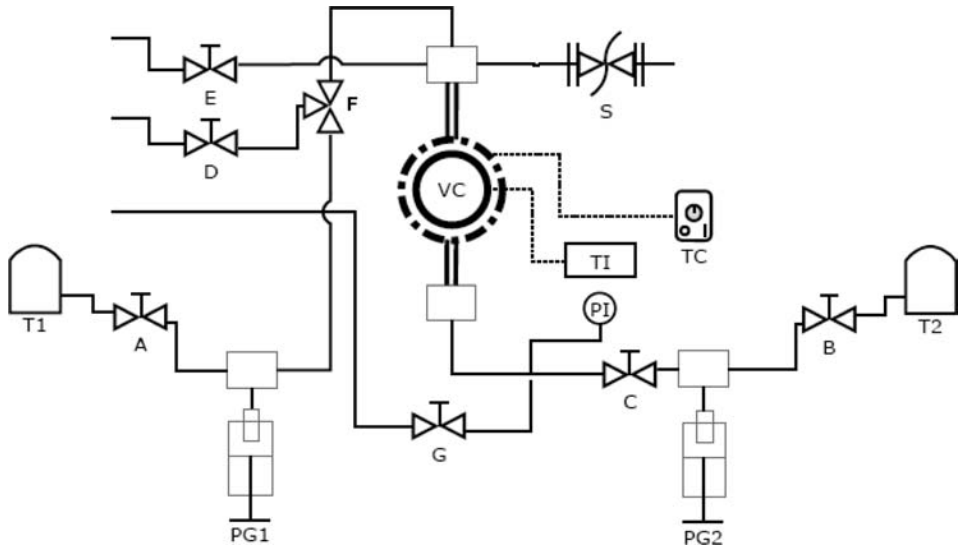

Figure 1. Flow diagram of the PD-E700 LL apparatus. In the diagram the following are annotated: view cell (VC); pressure transducer (PI); thermocouple (TI); temperature controller (TC); pressure generators (PG1 and PG2); liquid supply tanks (T1 and T2); valves (A−E); valve connecting to gas supply (G); and safety rupture disk (S). The dash-dotted line around the view cell indicates a heating jacket, and the double lines connecting to the view cell indicate 6.4 mm o.d. high-pressure tubing through which 1.6 mm o.d. capillary tubes reach into the view cell.

The temperature of the view cell was controlled with an electrical heating jacket which surrounded the vessel. The heating jacket was connected to a PID temperature controller, reading the temperature of the view cell by means of two (for safety) platinum resistance thermometers (PRT100). These PRTs were fitted in blind holes in the body of the view cell, in contact with a high-temperature thermally conductive paste. The temperature of the fluids was measured by means of a NiCr−Ni thermocouple that was fitted with a high-pressure connection within the view cell, directly in contact with the fluids. The overall temperature control had a stability of ± 0.1 K, and the overall uncertainty of the temperature was 0.2 K with a coverage factor $k = 2$. The pressure was monitored by means of a pressure transducer (Keller, model PA-33X, Winterthur, Switzerland) with an operating range up to $p = 100$ MPa. The transducer had a relative uncertainty of 0.1 % of the full scale up to $p =$ 70 MPa. A monochrome CCTV camera (Toshiba Teli, model CCD CS8420C-02, Tokyo, Japan) was used for monitoring the drops. The camera was connected to a frame grabber PCI board for image or video recording. To provide images with proper contrast, a white light emitting diode (LED) (Krüss GmbH, model DSA20B, Hamburg, Germany), fitted with a diffusion filter, was placed on the other end of the view cell, opposite to the camera. The interfacial tension was determined from digitized images of the drops by means of DSA software (Krüss GmbH, DSA V1.90.0.14, Hamburg, Germany). The o.d. of the capillary tube used for creating the pendant drops was measured to be 1.62 mm with an uncertainty of ± 0.01 mm. This diameter served as a calibration length for determining the dimensions of the pendant drops from the images recorded. Under the resolution of the camera used (767 × 575 pixels), the magnification factor of these images was approximately 70 pixels mm^{-1} depending on the distance of the camera from the drop. Each pixel at this magnification corresponded, therefore, to a physical size of $1/(70\ mm^{-1}) = 0.014$ mm, which is of the same order of magnitude as the uncertainty in the o.d. of the capillary tube. Thus determining its size more accurately would not reduce the overall uncertainty as the resolution is the limiting factor.

Experimental Procedure. The apparatus was thoroughly cleaned before use with appropriate solvents such as hexane, isopropanol, and/or toluene to dissolve any compounds remaining from previously conducted experiments. It was then drained, flushed with CO_2, and subsequently put under vacuum at a temperature of 323 K. This ensured that any remaining solvent was completely evaporated. All glassware was cleaned in concentrated KOH−isopropanol solution and was repeatedly rinsed with deionized H_2O before use. This ensured that no oil impurities would dissolve in the H_2O phase during handling. The view cell was then filled with CO_2. The left-hand pressure generator "PG1" was completely filled with H_2O and was kept isolated from the view cell with valve "F". Enough H_2O was introduced initially, until a H_2O phase was apparent in the lower side of the view cell, and time was allowed to ensure that the CO_2 bulk phase was saturated with H_2O. Valve "F" was thereafter opened only for allowing a H_2O drop to be created within the view cell and was immediately closed, isolating the unsaturated H_2O phase from the CO_2-rich phase. For every state point, four consecutive drops were created, and each was monitored for at least 600 s. The software was set to capture frames every 4 s which were all later analyzed for the calculation of the interfacial tension. After the creation of each drop, a transition period was observed during which the interfacial tension dropped rapidly and then stabilized at a "quasi-static value", similar to the observations of Hebach et al.[20] This initial time dependence is a common observation made by a number of authors[16,17,19,20,23,30] and is attributed to phase equilibration as the two phases partially dissolve in each other. As an example, the time evolution of the interfacial tension for different pressures at $T = 297.9$ K is shown in Figure 2.

Data Analysis. The relation[13] that describes the shape of a pendant drop is

$$\frac{d\phi}{ds} = 2k_{apex} - \left(\frac{z\Delta\rho g}{\gamma}\right) - \left(\frac{\sin\phi}{x}\right) \qquad (1)$$

where ϕ is the angle between the tangent at any point P on the profile of the drop and the horizontal axis, s is the respective arc length from the apex of the drop to the point P, k_{apex} is the curvature at the drop's apex, z is the height of point P from the horizontal axis, x is the distance of point P from the vertical axis, $\Delta\rho$ is the density difference between the two phases, and $g = 9.81\ m \cdot s^{-2}$ is the local gravitational acceleration. Equation 1 is derived by combining the Laplace equation of capillarity

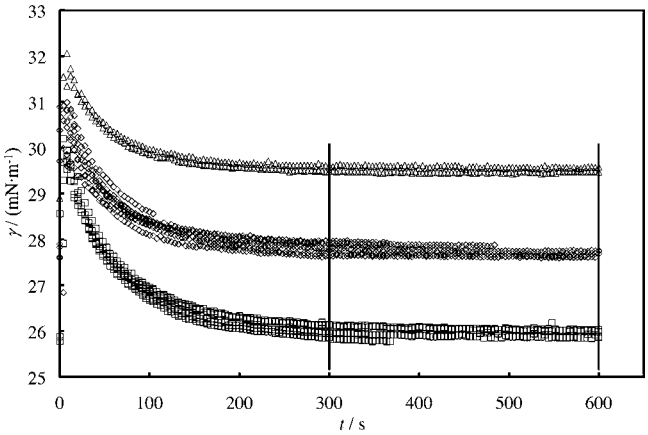

Figure 2. Interfacial tension measurements of the (H_2O + CO_2) system at 297.9 K as a function of time at different pressures: △, at 10.0 MPa; ◇, at 15.0 MPa; □, at 20.0 MPa. Vertical lines indicate the time interval over which all data points were used to get the average interfacial tension values.

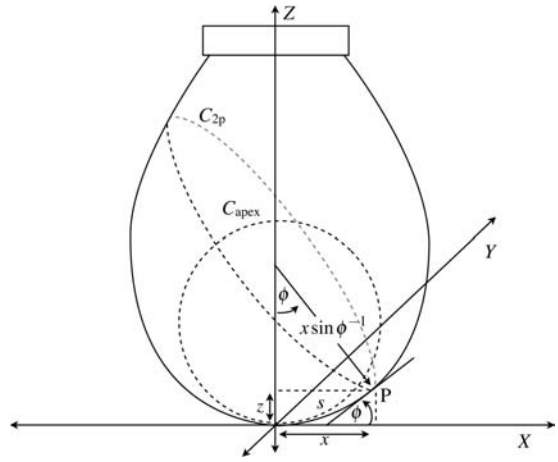

Figure 3. Pendant drop geometric representation showing *X*, *Y*, and *Z* as the origin axes, ϕ the angle between the tangent at any point P on the profile of the drop and the horizontal axis, *s* the respective arc length from the apex of the drop to point P, *z* the height of point P from the horizontal axis, *x* the distance of point P from the vertical axis, and C_{apex} and C_{2P} the circles of curvature at the apex and at point P, respectively. The curvature at the apex is the same at every direction due to symmetry, while that at point P is not. The total curvature at the apex is therefore $2k_{apex}$, while at point P the total curvature can be written as $k_{1P} + k_{2P} = d\phi/ds + \sin\phi/x$.

written for both the apex and a point P of the profile of the drop, with the pressure difference between the two points, given by $\Delta p_{apex} = 2\gamma k_{apex}$, $\Delta p_P = \gamma(k_{1P} + k_{2P})$, and $\Delta p_{apex} - \Delta p_P = z\Delta\rho g$, respectively. A geometric representation of a pendant drop where the above are illustrated is given in Figure 3.

Introducing the parameter $\alpha = (\gamma/\Delta\rho g)^{1/2}$ as the capillary constant in dimensions of length and $B = (\alpha k_{apex})^{-1}$ as the dimensionless drop form parameter, the relation describing the shape of a pendant drop may be expressed in reduced form as

$$\frac{d\phi}{dS} = \frac{2}{B} - Z - \frac{\sin\phi}{X} \tag{2}$$

where $X = x/\alpha$, $Z = z/\alpha$, and $S = s/\alpha$ are dimensionless variables. By rearranging the terms in the expression of *B*, its relation with the interfacial tension and the density difference of the two phases becomes

$$\gamma = \frac{\Delta\rho g}{(Bk_{apex})^2} \tag{3}$$

The density of CO_2 increases with pressure, generally, more rapidly than does the density of H_2O. This causes the density difference of the two phases to reduce with pressure, eventually leading to CO_2 becoming denser than H_2O. At low temperatures, this (isochoric point) appears within the pressure range of interest. In fact, assuming densities of the pure compounds at $T = 298$ K, CO_2 becomes denser than H_2O at pressures above 43.7 MPa.[31] This is the reason why the isotherm at $T = 297.9$ K does not extend in pressure, as for higher temperatures, both in this work and in the literature. Interfacial tension by the pendant drop method cannot be measured unless there is a density difference large enough to adequately elongate the drop, distorting it from being spherical (as would be the case in absence of gravity). For this isotherm the density difference, even if reversed, would remain in the range of (10 to 20) kg·m^{-3} for pressures up to 60 MPa which would make interfacial tension measurements of CO_2 pendant drops in H_2O bulk phase highly uncertain. The elongation of a pendant drop is quantified by *B* which should be in the range 0.7 to 0.8 for minimizing the sensitivity in interfacial tension determination to errors in the aspect ratio of the digital camera (see Song and Springer[13]). The aspect ratio of the digital camera used in the present work was equal to 1.00, as determined by calibration with a ball-bearing, and had a resolution of 767 × 575 pixels. For the (H_2O + CO_2) system, *B* decreases with decreasing density difference at constant temperature. In the present work, the extreme case of lowest density difference at $T = 333.5$ K and $p = 60$ MPa, was $\Delta\rho = 41$ kg·m^{-3}, where *B* has a value of 0.46 which is outside the preferred range leading to more uncertain results. Moreover, in this range the drop becomes much bigger in volume than at higher density difference, which creates practical problems in terms of focusing with the camera and the physically available space in the view cell. For comparison, the drop's volume for $\Delta\rho = 200$ kg·m^{-3} is only about 55 μL, while for $\Delta\rho = 41$ kg·m^{-3} it is of the order of 180 μL.

Results

Five isotherms have been measured for a range of pressures from (1 to 60) MPa, and the results are given in Table 2 and Figure 4. We observe that $|d\gamma/dp|$ is largest at low pressures and that it declines as the pressure increases. In fact, for the isotherms measured at T/K = 297.9, 312.9, and 333.5 the change in slope is abrupt, giving an indication of two distinct regions. The interfacial tension in the two regions of low and high pressure, corresponding for each isotherm to the gaseous and liquid or supercritical regions of CO_2, respectively ($T_c = 304.2$ K and $p_c = 7.38$ MPa), was fitted with an absolute average relative deviation of 1.4 % as linear functions of the form

$$\gamma/(\mathrm{mN\cdot m^{-1}}) = a_1 - b_1(p/\mathrm{MPa}) \tag{4}$$

where *p* is the pressure and a_1 and b_1 are fitting parameters.

The isotherms at $T = 343.3$ K and $T = 374.3$ K showed a more gradual change of slope with increasing pressure. These were fitted with a multiple multiplication factor (MMF) model of the form

$$\gamma/(\mathrm{mN\cdot m^{-1}}) = \frac{a_2 b_2 + c(p/\mathrm{MPa})^d}{b_2 + (p/\mathrm{MPa})^d} \tag{5}$$

where a_2, b_2, *c*, and *d* are fitting parameters. The parameters and correlation coefficients for both the linear fitting and the

Table 2. Interfacial Tension Results of the (H_2O + CO_2) System[a]

p/MPa	*T*/K	H_2O (1)	CO_2 (2)	$\Delta\rho$/kg·m^{-3}	γ/mN·m^{-1}
1.01	297.8	L	G	979	65.73 ± 0.27
2.00	297.9	L	G	958	58.90 ± 0.21
3.00	297.9	L	G	934	52.42 ± 0.36
4.00	297.9	L	G	906	47.02 ± 0.32
5.01	297.9	L	G	867	41.29 ± 0.20
6.01	297.9	L	G	804	36.00 ± 0.24
7.02	297.9	L	L	250	30.12 ± 0.11
8.02	297.9	L	L	221	30.28 ± 0.08
10.01	297.9	L	L	181	29.66 ± 0.20
14.99	297.9	L	L	126	27.73 ± 0.10
19.99	297.9	L	L	90	25.99 ± 0.09
1.00	312.9	L	G	975	63.55 ± 0.26
2.00	312.9	L	G	956	58.79 ± 0.27
3.01	312.8	L	G	935	51.15 ± 0.11
4.01	312.8	L	G	910	46.94 ± 0.27
5.02	312.8	L	G	881	43.93 ± 0.23
6.00	312.8	L	G	845	40.21 ± 0.17
7.02	312.9	L	G	796	36.87 ± 0.19
8.02	312.9	L	SC	715	33.47 ± 0.19
10.00	312.9	L	SC	363	31.20 ± 0.15
15.00	312.9	L	SC	216	29.17 ± 0.13
20.02	313.2	L	SC	161	28.33 ± 0.16
24.92	312.9	L	SC	124	27.14 ± 0.09
1.00	333.5	L	G	967	62.48 ± 0.33
1.99	333.5	L	G	950	59.93 ± 0.40
2.99	333.5	L	G	931	56.03 ± 0.26
3.99	333.5	L	G	910	52.42 ± 0.25
5.00	333.5	L	G	887	49.49 ± 0.22
6.00	333.5	L	G	861	46.28 ± 0.15
7.01	333.5	L	G	831	43.36 ± 0.12
8.01	333.5	L	SC	796	40.49 ± 0.08
8.99	333.5	L	SC	752	37.76 ± 0.18
10.00	333.6	L	SC	700	32.05 ± 0.27
10.57	333.6	L	SC	662	31.23 ± 0.24
15.01	333.5	L	SC	388	30.47 ± 0.15
20.00	333.5	L	SC	270	29.07 ± 0.07
25.00	333.5	L	SC	208	27.44 ± 0.17
30.00	333.5	L	SC	167	26.91 ± 0.12
40.00	333.5	L	SC	111	24.81 ± 0.11
50.00	333.5	L	SC	71	22.97 ± 0.16
60.00	333.5	L	SC	41	19.72 ± 0.03
1.00	343.3	L	G	962	61.28 ± 0.53
2.00	343.3	L	G	946	57.00 ± 0.27
3.00	343.3	L	G	928	55.58 ± 0.38
4.00	343.3	L	G	908	51.55 ± 0.17
5.00	343.3	L	G	887	48.50 ± 0.20
6.00	343.3	L	G	864	45.36 ± 0.23
7.05	343.3	L	G	837	42.49 ± 0.18
8.03	343.3	L	SC	808	39.83 ± 0.30
9.02	343.3	L	SC	774	37.46 ± 0.17
10.03	343.3	L	SC	735	35.38 ± 0.25
11.04	343.3	L	SC	687	33.97 ± 0.16
12.05	343.3	L	SC	637	32.75 ± 0.19
15.09	343.3	L	SC	476	30.31 ± 0.15
20.20	343.3	L	SC	324	28.36 ± 0.12
25.25	343.3	L	SC	249	27.46 ± 0.08
35.28	343.3	L	SC	165	25.52 ± 0.12
41.32	343.3	L	SC	132	24.41 ± 0.14
1.00	374.3	L	G	944	56.20 ± 0.50
2.00	374.3	L	G	929	53.44 ± 0.40
3.00	374.3	L	G	913	51.23 ± 0.25
4.00	374.3	L	G	897	48.76 ± 0.08
5.00	374.3	L	G	880	46.53 ± 0.09
6.00	374.3	L	G	861	44.64 ± 0.13
9.00	374.3	L	SC	799	39.67 ± 0.04
10.00	374.3	L	SC	775	38.05 ± 0.25
11.00	374.3	L	SC	750	36.64 ± 0.16
12.00	374.3	L	SC	723	35.05 ± 0.37
13.00	374.3	L	SC	695	33.81 ± 0.50
14.00	374.3	L	SC	666	32.81 ± 0.32
15.00	374.3	L	SC	636	32.22 ± 0.37
16.00	374.3	L	SC	605	31.21 ± 0.39
17.00	374.3	L	SC	575	30.45 ± 0.23
18.00	374.3	L	SC	546	29.92 ± 0.26
19.00	374.3	L	SC	517	29.27 ± 0.34
20.00	374.3	L	SC	491	29.13 ± 0.17
30.00	374.3	L	SC	314	25.27 ± 0.13
40.00	374.3	L	SC	227	24.04 ± 0.10
49.99	374.3	L	SC	164	22.25 ± 0.11
60.05	374.3	L	SC	121	21.23 ± 0.04

[a] The errors correspond to the standard deviation of the interfacial tension data, calculated for all frames recorded between the fifth and tenth minutes after the creation of each drop, for four consecutive drops at each state point. The density difference used for the determination of the interfacial tension at each state point corresponds to that between the pure compounds of H_2O (1) and CO_2 (2) with their respective phase states indicated as G = gaseous, L = liquid, or SC = supercritical.

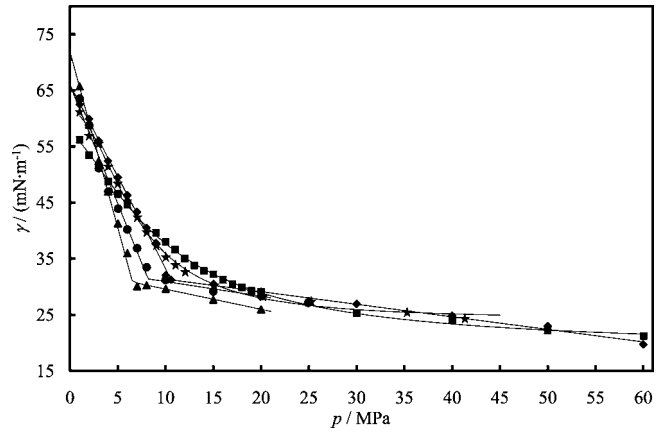

Figure 4. Interfacial tension measurements of the (H_2O + CO_2) system as a function of pressure at different isotherms: ▲, at 297.9 K; ●, at 312.9 K; ◆, at 333.5 K; ★, at 343.3 K; and ■, at 373.3 K.

Table 3. Fitting Parameters of the Interfacial Tension Results for the (H_2O + CO_2) System[a]

dual linear correlation									
$p \le p_i$					$p \ge p_i$				
T/K	a_1	b_1	σ	$10^2\ \Delta_{AAD}$	p_i/MPa	a_1	b_1	σ	$10^2\ \Delta_{AAD}$
297.9	71.842	6.266	1.0784	1.63	6.548	33.171	0.360	0.3100	0.46
312.9	65.928	4.227	1.6670	2.77	8.169	33.537	0.262	0.3776	0.74
333.5	65.963	3.266	0.6732	1.17	10.641	33.595	0.224	0.4289	1.22

multiple multiplicative model (eq 5)						
T/K	a_2	b_2	*c*	*d*	σ	$10^2\ \Delta_{AAD}$
343.3	24.100	0.022	61.283	−1.996	0.6073	1.13
374.3	19.056	0.037	57.258	−1.452	0.3150	0.72

[a] p_i values correspond to the intersection pressure of the two lines for each isotherm in the dual linear fitting. The absolute average deviation and the standard error were calculated by $\Delta_{AAD} = \sum_{i=1}^{N}|(\gamma_i - \gamma_f)/(\gamma_i)|/N$ and $\sigma^2 = \sum(\gamma_i - \gamma_f)^2/(j - n)$, respectively, where γ_i is the measured interfacial tension at each state point, γ_f is the corresponding fitted interfacial tension, $\bar{\gamma}$ is the average measured interfacial tension, *j* is the number of state points, and *n* is the number of fitting parameters.

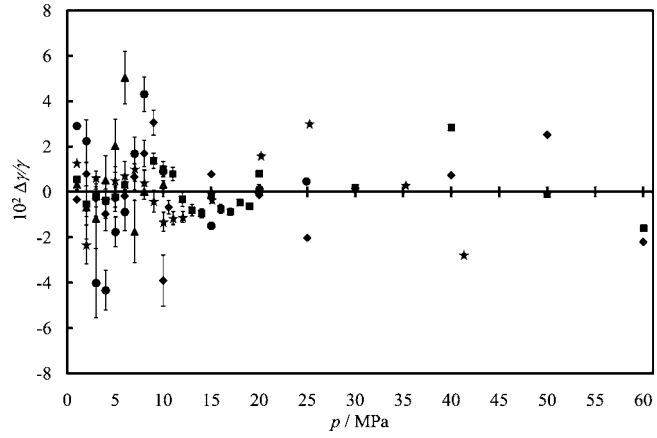

Figure 5. Difference of interfacial tension measurements of the (H_2O + CO_2) system from the fitting equations as a function of pressure at different isotherms. Error bars correspond to the combined standard uncertainty of pressure and temperature readings with a coverage factor $k = 2$: ▲, at 297.9 K; ●, at 312.9 K; ◆, at 333.5 K; ★, at 343.3 K; and ■, at 373.3 K.

MMF model are given in Table 3. The deviation of the data from these correlation curves is shown in Figure 5. The maximum absolute relative deviation is 5.0 %, and the average absolute relative deviation is 1.2 %.

The interfacial tension shows a small positive dependence on temperature at pressures above 15 MPa, while at lower

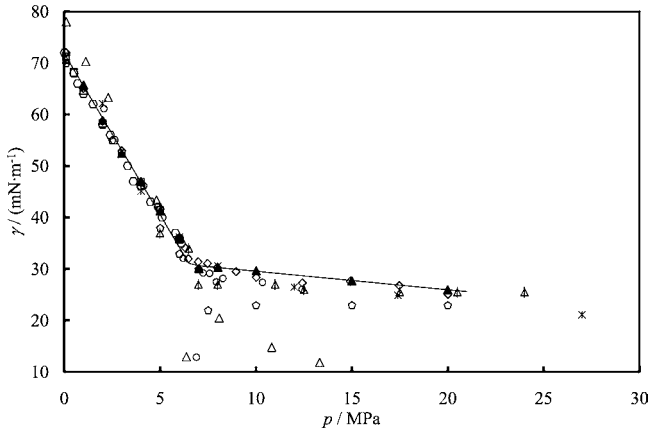

Figure 6. Interfacial tension of the ($H_2O + CO_2$) system as a function of pressure compared to literature values: present work, ▲, at 297.9 K; Jho et al.,[39] ⬡, at 298.16 K; Massoudi and King,[27] □, at 298.15 K; Chun and Wilkinson,[18] ○, at 298.15 K; Wesch et al.,[40] ⬠, at 298.00 K; Hebach et al.,[20] ◇, at 298.30 K; Park et al.,[23] △, at 298.15 K; Chalbaud et al.,[19] ⏃, at 300.15 K; and Bachu and Bennion,[26] ∗, at 298.15 K. For Jho et al.,[39] Wesch et al.,[40] and Chalbaud et al.[19] the data points were inferred from graphs.

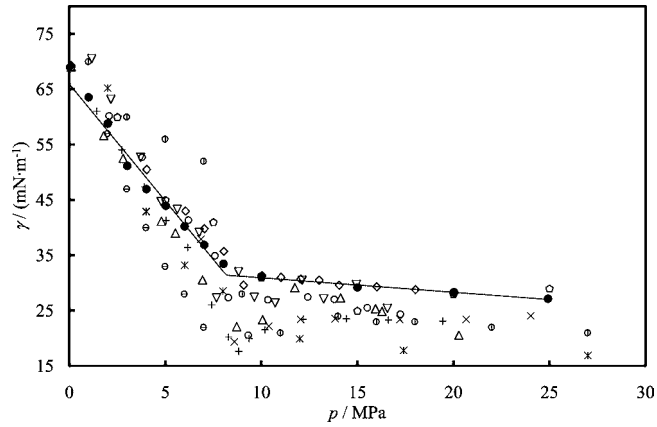

Figure 7. Interfacial tension of the ($H_2O + CO_2$) system as a function of pressure compared to literature values: present work, ●, at 312.9 K; Hough et al.,[41] +, at 311.15 K; Chun and Wilkinson,[18] ○, at 311.20 K; Wesch et al.,[40] ⬠, at 313.00 K; da Rocha et al.,[17] ×, at 311.15 K; Hebach et al.,[20] ◇, at 318.4 K; Tewes et al.,[16] ⊖, at 313.15 K; Park et al.,[23] △, at 311.15 K; Akutsu et al.,[24] ▽, at 318.15 K; Sutjiadi-Sia et al.,[30] ⌀, at 313 K; and Bachu and Bennion,[26] ∗, at 314.15 K. For Wesch et al.,[40] Tewes et al.,[16] and Sutjiadi-Sia et al.[30] the data points were inferred from graphs. For Hough et al.[41] and da Rocha et al.[17] the data were taken from Park et al.[23]

pressures, an increase in temperature has the opposite effect, reducing the interfacial tension. A crossover between the isotherms is observed at a pressure of approximately 4 MPa, where the interfacial tension shows the smallest sensitivity to temperature.

The uncertainty of the interfacial tension associated with the uncertainties in pressure and temperature is given by (from Taylor et al.[32])

$$u_c^2(\gamma) = \left(\frac{\partial \gamma}{\partial p}\right)^2 u^2(p) + \left(\frac{\partial \gamma}{\partial T}\right)^2 u^2(T) \qquad (6)$$

where u_c is the combined standard uncertainty, $u(p) = 5 \cdot 10^{-4} p$ is the uncertainty in pressure, and $u(T) = 0.1$ K is the uncertainty in temperature.

The average interfacial tension values reported were obtained from all of the frames recorded between the fifth and the tenth minutes after creating the drop, for four consecutive drops at each state point. The results for individual isotherms are shown in Figures 6 to 10 in comparison with data from other authors. The density difference between the two phases was assumed to be that between the pure compounds at each state point, and density values were obtained from models given in the National Institute of Standards and Technology Chemistry Webbook.[31]

The standard errors of the interfacial tension reported were obtained from the average values calculated from all drop frames under consideration. Approximately 200 drop frames were used to evaluate the interfacial tension at each state point. The number of measurements is substantial, the standard error of which includes additional experimental errors such as the effect of vibrations and errors associated with the DSA as well as the reproducibility of the measurement. The average relative standard error of all measurements is 0.5 % and reaches a maximum of 1.5 % at 373.3 K and 13 MPa. This statistical standard error overlaps to some extent with the uncertainties in p and T. The combined standard uncertainty u_c, associated with $u(p)$ and $u(T)$ with a coverage factor $k = 2$ (confidence greater than 95 %) as calculated with eq 6, has an average relative value of 0.4 % and reaches a maximum of 1.5 % at 312.9 K and 3 MPa.

The values of interfacial tension obtained from DSA are linearly dependent on the density difference of the two fluids.

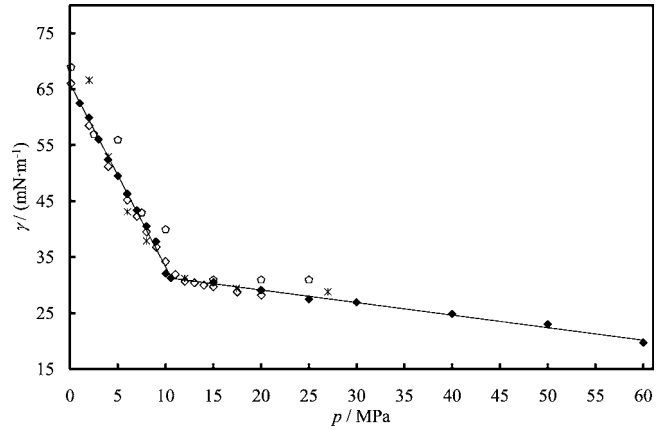

Figure 8. Interfacial tension of the ($H_2O + CO_2$) system as a function of pressure compared to literature values: present work, ◆, at 333.5 K; Wesch et al.,[40] ⬠, at 333.00 K; Hebach et al.,[20] ◇, at 333.2 K; and Bachu and Bennion,[26] ∗, at 333.15 K. For Wesch et al.[40] the data points were inferred from graphs.

The values of density difference used for the calculation of the interfacial tension are given in Table 2, allowing for future corrections. If measurements or models reveal that the density difference is significantly different from the values used, then the values of interfacial tension reported here may be corrected by multiplying with the ratio of the new density difference over the one used in the present work. Simultaneous density and interfacial tension measurements at elevated pressures and temperatures, however, increases the complexity of a pendant drop apparatus and introduces further measuring uncertainties (see Chiquet et al.[25] and Bachu and Bennion[26]).

Discussion

The dependence of interfacial tension upon pressure can readily be linked to the isothermal compressibility, β, of the two phases. In fact, for the three isotherms where the interfacial tension was fitted using two linear regions for low and high pressure, the intersection points of the fitting lines coincide with the pressures at which the compressibility of pure CO_2 reaches a local maximum, β_{max}, for each particular temperature. For T

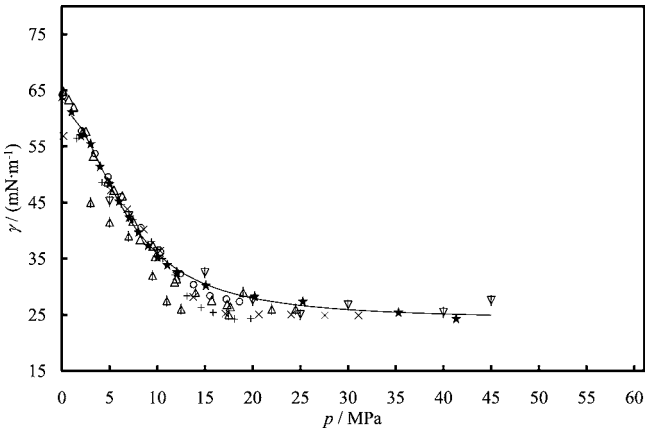

Figure 9. Interfacial tension of the (H_2O + CO_2) system as a function of pressure compared to literature values: present work, ★, at 343.3 K; Hough et al.,[41] +, at 344.15 K; Chun and Wilkinson,[18] ○, at 344.20 K; da Rocha et al.,[17] ×, at 344.15 K; Park et al.,[23] △, at 344.15 K; Chiquet et al.,[25] ▽, at 343 K; and Chalbaud et al.,[19] ◭, at 344.15 K. For Hough et al.[41] and da Rocha et al.[17] the data were taken from Park et al.[23]

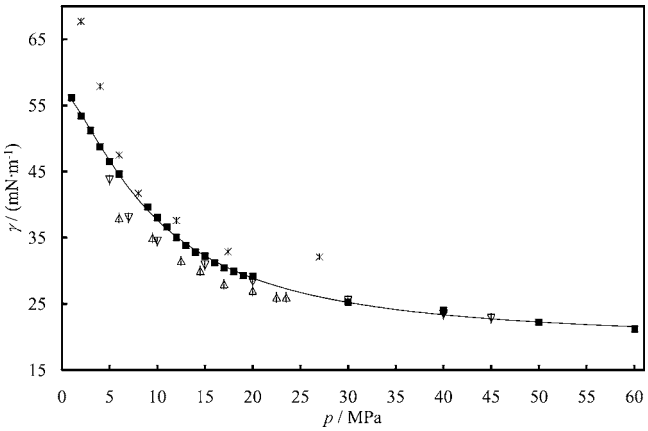

Figure 10. Interfacial tension of the (H_2O + CO_2) system as a function of pressure compared to literature values: present work, ■, at 373.3 K; Chiquet et al.,[25] ▽, at 383 K; Chalbaud et al.,[19] ◭, at 373.15 K; and Bachu and Bennion,[26] ∗, at 373.15 K. For Chalbaud et al.[19] the data points were inferred from graphs.

= 297.9 K, β_{max} = 0.75 MPa^{-1} at p = 6.4 MPa which corresponds to the phase change of CO_2 from gas to liquid.[31] The two fitting lines on this isotherm intersect at a same pressure (see Table 3). For T = 312.9 K and T = 333.5 K the local maximum compressibility is (0.71 and 0.21) MPa^{-1} at approximately p = 8.75 MPa and p = 10.4 MPa, respectively, which is also very close to the intersection values of the two fitting lines. The compressibility of CO_2 has a direct influence on the free energy density and therefore upon the interfacial tension of the binary system in which, by comparison, H_2O is virtually incompressible.[17] The influence of the free energy density of the two phases as well as information on different modeling approaches of interfacial properties can be found in the literature.[33−36]

The interfacial tension values of the present work are in reasonable agreement with the values reported by Chiquet et al.,[25] Massoudi and King,[27] and Hebach et al.[20] but extend the available data to higher pressures. The scatter of published values and differences from the current values (see Figures 6 to 10) are mainly in the range of higher densities of the CO_2-rich phase. For the gaseous states of CO_2, better agreement with the literature values is seen than with values for the liquid or supercritical states of CO_2 (see Table 1). Although these

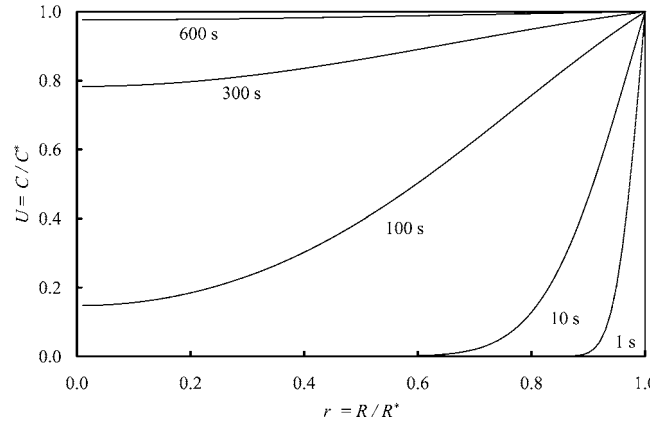

Figure 11. Concentration distribution of CO_2 in a H_2O spherical drop of R^* = 0:2 cm at t = 1 s, t = 10 s, t = 100 s, t = 300 s, and t = 600 s.

discrepancies have been attributed in the literature to different approaches in the two-phase equilibration and in the density difference determination, we attribute them to surfactant effects. Surface active impurities are unavoidably present in any high-pressure apparatus[37] and can decrease interfacial tension values, especially at conditions of higher CO_2-rich phase densities, as for the liquid or supercritical regions. In fact, Park et al.,[23] Tewes and Boury,[16] Akutsu et al.,[24] and da Rocha et al.[17] have measured the influence of surfactants on the interfacial tension of the (H_2O + CO_2) system. Surfactant migration to the H_2O drop could also explain the long-term "aging" effects expected for the system as suggested by Hebach et al.[20] The time scales, as well as the conditions where the major disagreements in literature values appear, point to this possible explanation.

The initial time dependence of the interfacial tension in the first few minutes, following the creation of a drop, has been associated with the time required to reach phase equilibrium with the surrounding fluid. Assuming that this process is controlled by diffusion within the drop, the time required to attain equilibrium may be estimated by solving the differential equation describing one-dimensional diffusion of a solute into a spherical liquid drop given by

$$\frac{\partial u(r,t)}{\partial t} = D^*\frac{2}{r}\frac{\partial u(r,t)}{\partial r} + D^*\frac{\partial^2 u(r,t)}{\partial r^2} \qquad (7)$$

where $u(r, t) = C/C^*$ is the reduced concentration of the fluid in the liquid with C^* the solubility at each state point, $r = R/R^*$ is the reduced radial variable with R^* the radius of the drop, and $D^* = D/R^{*2}$ is the reduced diffusion coefficient. The analytical solution for the differential eq 7, subject to boundary and initial conditions $u(1, t) = 1$, $u(0, t)$ = finite, and $u(r, 0) = m(r)$, is

$$u(r,t) = 1 + \frac{2(1-m(r))}{r}\sum_{n=1}^{n}\frac{1}{n\pi}\cos(n\pi) \times \exp(-n^2\pi^2 D^* t)\sin(n\pi r) \qquad (8)$$

where $m(r)$ is a spatial function giving the initial concentration of the fluid in the drop. Assuming the initial concentration profile to be $m(r) = 0$, the diffusion coefficient of CO_2 in H_2O[38] to be $D = 3\cdot10^{-9}$ $m^2\cdot s^{-1}$, and a drop radius R^* = 2 mm (a representative size of H_2O pendant drops in CO_2), the reduced diffusion coefficient is $D^* = 7.5\cdot10^{-4}$ s^{-1}. The solution is shown in Figure 11, for spatial concentration distributions of CO_2 in the H_2O spherical drop, at different times between (1 and 600) s. Under this numerical validation, it is observed that the concentration of CO_2 reaches

approximate equilibrium within 300 s, while after 600 s it is virtually uniform. Effects from saturation processes at such length scales must, therefore, be associated with a hundreds of seconds order of magnitude and not greater.

Conclusions

Interfacial tension measurements have been made for the (H_2O + CO_2) system on five isotherms from $T = 297.9$ K to $T = 374.3$ K at pressures up to $p = 60$ MPa. The data have been fitted as a function of pressure by correlating equations for each isotherm with a maximum absolute relative deviation of 5.0 % and an average absolute relative deviation of 1.2 % (see Figure 5). The relative standard errors reported are in most cases less than 1.0 %. These were derived from a large number of experimental values collected for each state point. Good agreement with previous literature values was seen under conditions where CO_2 is a gas, while at higher bulk densities most previous data showed significant disagreement and were usually smaller than the ones reported in this work. Possible reasons for these discrepancies have been suggested. Measurements of interfacial tension for the (H_2O + CO_2) system at conditions relevant to EOR and carbon storage have been completed as a first step toward more realistic modeling of such processes.

Literature Cited

(1) IPCC. *Climate Change 2001: The Scientific Basis*; Cambridge University Press: New York, 2001.
(2) IPCC. *Climate Change 2007: Synthesis Report*; IPCC: New York, 2007.
(3) IPCC. *Special Report on Carbon Dioxide Capture and Storage*; Cambridge University Press: New York, 2005.
(4) Gibbins, J.; Chalmers, H. Carbon Capture and Storage. *Energy Policy* **2008**, *36*, 4317–4322.
(5) Bruant, R. G., Jr.; Guswa, A. J.; Celia, M. A.; Peters, C. A. Safe Storage of CO_2 in Deep Saline Aquifers. *Environ. Sci. Technol.* **2002**, *36*, 240A–245A.
(6) Span, R.; Wagner, W. A New Equation of State for Carbon Dioxide Covering the Fluid Region from the Triple-Point Temperature to 1100 K and Pressures up to 800 MPa. *J. Phys. Chem. Ref. Data* **1996**, *25*, 1509–1596.
(7) Tamburri, M. N.; Peltzer, E. T.; Friederich, G. E.; Aya, I.; Yamane, K.; Brewer, P. G. A Field Study of the Effects of CO_2 Ocean Disposal on Mobile Deep-Sea Animals. *Mar. Chem.* **2000**, *72*, 95–101.
(8) Brewer, P. G.; Friederich, G.; Peltzer, E. T.; Orr, F. M., Jr. Direct Experiments on the Ocean Disposal of Fossil Fuel CO_2. *Science* **1999**, *284*, 943–945.
(9) Haugan, P. M.; Drange, H. Effects of CO_2 on the Ocean Environment. *Energy Convers. Manage.* **1996**, *37*, 1019–1022.
(10) Blunt, M.; Fayers, F. J.; Orr, F. M., Jr. Carbon Dioxide in Enhanced Oil Recovery. *Energy Convers. Manage.* **1993**, *34*, 1197–1204.
(11) Qi, R.; LaForce, T. C.; Blunt, M. J. Design of Carbon Dioxide Storage in Oilfields. *SPE Annual Technical Conference and Exhibition*, Sept 21−24, 2008, Denver, Colorado.
(12) Andreas, J. M.; Hauser, E. A.; Tucker, W. B. Boundary Tension by Pendant Drops. *J. Phys. Chem.* **1938**, *42*, 1001–1019.
(13) Song, B.; Springer, J. Determination of Interfacial Tension from the Profile of a Pendant Drop Using Computer-Aided Image Processing 1. Theoretical. *J. Colloid Interface Sci.* **1996**, *184*, 64–76.
(14) Adamson, A. W.; Gast, A. P. *Physical Chemistry of Surfaces*, 6th ed.; Wiley: New York, 1997.
(15) Song, B.; Springer, J. Determination of Interfacial Tension From the Profile of a Pendant Drop Using Computer-Aided Image Processing 2. Experimental. *J. Colloid Interface Sci.* **1996**, *184*, 77–91.
(16) Tewes, F.; Boury, F. Thermodynamic and Dynamic Interfacial Properties of Binary Carbon Dioxide−Water Systems. *J. Phys. Chem. B* **2004**, *108*, 2405–2412.
(17) da Rocha, S. R. P.; Harrison, K. L.; Johnston, K. P. Effect of Surfactants on the Interfacial Tension and Emulsion Formation Between Water and Carbon Dioxide. *Langmuir* **1999**, *15*, 419–428.
(18) Chun, B. S.; Wilkinson, G. T. Interfacial Tension in High-Pressure Carbon Dioxide Mixtures. *Ind. Eng. Chem. Res.* **1995**, *34*, 4371–4377.
(19) Chalbaud, C.; Robin, M.; Lombard, J.-M.; Martin, F.; Egermann, P.; Bertin, H. Interfacial Tension Measurements and Wettability Evaluation for Geological CO_2 Storage. *Adv. Water Res.* **2009**, *32*, 98–109.
(20) Hebach, A.; Oberhof, A.; Dahmen, N.; Kögel, A.; Ederer, H.; Dinjus, E. Interfacial Tension at Elevated Pressures−Measurements and Correlations in the Water + Carbon Dioxide System. *J. Chem. Eng. Data* **2002**, *47*, 1540–1546.
(21) Zappe, J.; Wesch, A.; Ebert, K. H. Measurement of the Mass Transfer into Single Drops in the System of Water/Supercritical Carbon Dioxide. *J. Colloid Interface Sci.* **2000**, *231*, 1–7.
(22) Kögel, A. Ph.D. Thesis. Forschungzentrum Karlsruhe GmbH, 2000.
(23) Park, J.-Y.; Lim, J. S.; Yoon, C. H.; Lee, C. H.; Park, K. P. Effect of a Fluorinated Sodium Bis(2-Ethylhexyl) Sulfosuccinate (Aerosol-OT, AOT) Analogue Surfactant on the Interfacial Tension of CO_2 + Water and CO_2 + Ni-Plating Solution in Near- and Supercritical CO_2. *J. Chem. Eng. Data* **2005**, *50*, 299–308.
(24) Akutsu, T.; Yamaji, Y.; Yamaguchi, H.; Watanabe, M.; Smith, R. L., Jr.; Inomata, H. Interfacial Tension Between Water and High Pressure CO_2 in the Presence of Hydrocarbon Surfactants. *Fluid Phase Equilib.* **2007**, *257*, 163–168.
(25) Chiquet, P.; Daridon, J.-L.; Broseta, D.; Thibeau, S. CO_2/Water Interfacial Tensions Under Pressure and Temperature Conditions of CO_2 Geological Storage. *Energy Convers. Manage.* **2007**, *48*, 736–744.
(26) Bachu, S.; Bennion, D. B. Interfacial Tension between CO_2, Freshwater, and Brine in the Range of Pressure from (2 to 27) MPa, Temperature from (20 to 125) °C, and Water Salinity from (0 to 334 000) $mg \cdot L^{-1}$. *J. Chem. Eng. Data* **2009**, *54*, 765–775.
(27) Massoudi, R.; King, A. D., Jr. Effect of Pressure on Surface Tension of Water Adsorption of Low Molecular Weight Gases on Water at 25 Degrees. *J. Phys. Chem.* **1974**, *78*, 2262–2266.
(28) Poulter, T. C. Apparatus for Optical Studies at High Pressure. *Phys. Rev.* **1932**, *40*, 860–871.
(29) Bridgman, P. W. *The Physics of High Pressure*; Bell and Sons: London, 1958.
(30) Sutjiadi-Sia, Y.; Jaeger, P.; Eggers, R. Interfacial Phenomena of Aqueous Systems in Dense Carbon Dioxide. *J. Supercrit. Fluids* **2008**, *46*, 272–279.
(31) *NIST Chemistry WebBook*, NIST Standard Reference Database Number 69; NIST: Gaithersburg, MD, 2008.
(32) Taylor, B. N.; Kuyatt, C. E. *Guidelines for Evaluating and Expressing the Uncertainty of NIST Measurement Results*; NIST: Gaithersburg, MD, 1994.
(33) Macleod, D. B. On a Relation Between Surface Tension and Density. *Trans. Faraday Soc.* **1923**, *19*, 38–41.
(34) Guggenheim, E. A. The Principle of Corresponding States. *J. Chem. Phys.* **1945**, *13*, 253–261.
(35) Cahn, J. W.; Hilliard, J. E. Free Energy of a Nonuniform System. I. Interfacial Free Energy. *J. Chem. Phys.* **1958**, *28*, 258–267.
(36) Gloor, G. J.; Jackson, G.; Blas, F. J.; del Río, E. M.; de Miguel, E. An Accurate Density Functional Theory for the Vapor-Liquid Interface of Associating Chain Molecules Based on the Statistical Associating Fluid Theory for Potentials of Variable Range. *J. Chem. Phys.* **2004**, *121*, 12740–12759.
(37) Susnar, S. S.; Hamza, H. A.; Neumann, A. W. Pressure Dependence of Interfacial Tension of Hydrocarbon−Water Systems Using Axisymmetric Drop Shape Analysis. *Colloids Surf., A* **1994**, *89*, 169–180.
(38) Frank, M. J. W.; Kuipers, J. A. M.; van Swaaij, W. P. M. Diffusion Coefficients and Viscosities of CO_2 + H_2O, CO_2 + CH_3OH, NH_3 + H_2O, and NH_3 + CH_3OH Liquid Mixtures. *J. Chem. Eng. Data* **1996**, *41*, 297–302.
(39) Jho, C.; Nealon, D.; Shogbola, S.; King, A. D., Jr. Effect of Pressure on Surface Tension of Water: Adsorption of Hydrocarbon Gases and Carbon Dioxide on Water at Temperatures Between 0 and 50 °C. *J. Colloid Interface Sci.* **1978**, *65*, 141–154.
(40) Wesch, A.; Dahmen, N.; Ebert, K.; Schön, J. Grenzflächenspannungen, Tropfengrössen und Kontaktwinkel im Zweiphasensystem H_2O/CO_2 bei Temperaturen von 298 bis 333 K und Drücken bis 30 MPa. *Chem. Ing. Tech.* **1997**, *69*, 942–946.
(41) Hough, E. W.; Heuer, G. J.; Walker, J. W. An Improved Pendant Drop, Interfacial Tension Apparatus and Data for Carbon Dioxide and Water. *Pet. Trans. AIME* **1959**, *216*, 469–472.

Received for review March 8, 2010. Accepted April 22, 2010. This work was carried out as part of the Imperial College−Shell Grand Challenge Programme on Clean Fossil Fuels. The authors gratefully acknowledge Shell International Exploration and Production B.V. for supporting the present project and for permission to publish this research. We also acknowledge the support of the Royal Society for a small research grant, which allowed the purchase of the high-pressure apparatus.

JE100198G